https://doi.org/10.1016/j.fuel.2020.118101

Theoretical chemical kinetics for catalytic pyrolysis of methyl acetate over H-ZSM-5 zeolites

Qinghui Meng[a,b], Beibei Feng[a] , Lidong Zhang[a,*], Peng Zhang [b,*], Liusi Sheng[a]

[a]*National Synchrotron Radiation Laboratory, University of Science and Technology of China, Hefei, Anhui 230029, P. R. China*

[b]*Department of Mechanical Engineering, the Hong Kong Polytechnic University, Hung Hom, Kowloon, Hong Kong*

Corresponding Author:
Lidong Zhang
National Synchrotron Radiation Laboratory
University of Science and Technology of China
Hefei, Anhui 230029, P.R. China
E-mail: zld@ustc.edu.cn
Fax: (86) 551 65141078 Tel: (86) 551 63607923

Peng Zhang
Department of Mechanical Engineering
The Hong Kong Polytechnic University
Kowloon, Hong Kong
E-mail: pengzhang.zhang@polyu.edu.hk
Fax: (852)23654703 Tel: (852)27666664

Abstract: The catalytic chemistry of methyl acetate (MA) over zeolites of great guidance in energy supply, environmental protection and industrial applications, has been investigated systematically and thoroughly by using calculations at the M06-2X/6-311++G(d,p) level of theory and its chemical reaction rate constants were calculated by using the transition state theory. Feasible reactions of the protolytic cracking channels are of particular interest in the present study, and results revealed that the ketene formation in the concerted mechanism and that of acetyloxy + CH_3 are competitive reactions during MA consumption. Furthermore, comparisons between the catalytic and conventional pyrolysis of MA were carried out to demonstrate the benefits introduced by the catalysts in MA combustion. It is demonstrated that the energy barriers of the dissociation reactions for MA over H-ZSM-5 zeolites decrease significantly with respect to the conventional pyrolysis of MA, which causes the change of production distribution. This work provides new insight into the mechanism of the MA catalytic pyrolysis that will guide the improvements in the engine combustion efficiency and in the control of volatile organic compounds, and will also help to improve the selectivity of the conversion of methanol to hydrocarbon and olefin products.

Key words: Methyl acetate, Biodiesels, Catalytic combustion, Ketene.

1. Introduction

Biodiesel is believed to be one of the most promising alternative fuels due to its attractive physical properties similar to fossil fuels and its potential to environmental protection. Biodiesel is generally composed of a mixture of extended alkyl chain methyl esters, which are typically derived from chemically reacting lipids with an alcohol through trans-esterification reactions [1, 2]. In addition, esters are oxygenated volatile organic compounds (VOC) that are of commercial interest as potential replacements for industrial solvent, of which the increased release will affect air quality seriously. It has been recognized that catalytic reactions of fuels with low concentrations occur at much lower oxidation temperatures, greatly diminishing the overall NO_x. Thus, the catalytic chemistry of esters is instructive for combustion and atmospheric chemistry of biodiesel.

Among biodiesel surrogates, methyl acetate (MA), the smallest ester with an alkyl backbone, is the least reactive species of C1-C4 methyl esters according to their autoignition delay times[3, 4]. Although MA is too short to exhibit the NTC behavior, it is still a desirable surrogate to study the characteristic properties of biodiesels. Many kinetic studies on MA, particularly on its hydrogen abstraction reactions and its low-temperature oxidation and pyrolysis reactions, have been conducted [5-7] since the first experiment performed by Dagaut et al. [8] in a jet-stirred reactor. The earlier studies on the pyrolysis of MA showed conflicting results regarding the main dissociation pathways [9, 10]. Based on the previous results of Peukert et al. [11] and Farooq et al. [12], Annesley et al. [13] identified dissociation pathways for MA in a diaphragmless shock tube using laser Schlieren densitometry and resolved the previous discrepancy on MA dissociations[9, 10].

Catalytic chemistry of MA has been proven to be critical for the for the formation of C-C bonds in the conversion processes of methanol to olefins (MTO), where ketene, the dissociation product of

MA, was verified to play a critical role in controlling selectivity [14, 15]. Efforts were called for figuring out the mechanism of ketene formation in order to either accelerate or suppress the ketene formation to obtain much more selective processes [16].

To our best knowledge, studies on MA conversion over catalytic sieves are scarcely available in literatures. Xu et al. [17] conducted a theoretical study on the activation of MA on Pd(111), which is used to understand the factors controlling the selectivity of ester hydrogenolysis. It revealed that the C–O bonds of MA (Ea $\approx$ 2.0 eV for the carbonyl and acetate-methyl bonds; Ea = 1.0 eV for the acetyl-methoxy bond) are much more difficult to dissociate than the C–H bonds. Romotowski et al. [18] investigated the interaction of MA with H-ZSM-5 using infrared spectroscopy. Their results suggested that MA interacts with H-ZSM-5 to produce acetic acid and methoxy species, and that the acetic acid further reacts with H-ZSM-5 to produce acetate and acylium ions. The C=O group with an effective hydrogen index of 0.67 makes MA a "hydrogen-deficient" chemical compound [19], which also gives rise to the highly exothermic reactions of the conversion of MA over catalysts. However, ketene is a highly reactive intermediate and cannot be detected in the infrared spectra.

To improve our understanding of the catalytic dissociation of MA and identify the formation of ketene intermediates, we theoretically elucidated the evolution pathway of MA dissociation over H-ZSM-5 zeolites in the current study. We shall discuss the catalytic dissociation reactions that can be used to deduce the likelihood with which certain reaction channels are energetically favorable from the corresponding energy barriers. Furthermore, we shall determine the energy barrier decreases of these catalytic pyrolysis reactions of MA compared with those in direct pyrolysis of MA. These energy barrier decreases are responsible for the significant reduction of the ignition temperature, leading to less emission and higher combustion efficiency.

2. Computational methods

2.1 Catalyst Model

ZSM-5 with medium pore size is a high silica zeolite with a two-dimensional interconnected 10-ring channel system, which is highly favorable for shape selectivity [20]. The Bronsted acid site of the H-ZSM-5 zeolites exhibiting distinct zeolitic environments was created by substituting the silicon atom with the aluminum atom and adding a proton on the adjacent oxygen atom. It was reported that the aluminum atom cannot be located precisely because the energies of its substitution at different tetrahedral sites differ very slightly from each other, and that comparisons between the calculated NMR shifts and experimental spectra are not yet as accurate as required for the accurate location of the aluminum atom. Previous theoretical studies have found that the T12 site is the preferred location for the aluminum atom, where the Bronsted acid site accesses the adsorbed molecules with the highest probability in both the straight and zigzag channels and could accommodate larger species [21]. Thus, the T12 site is the common choice for the replacement of Si by Al in computational investigations of adsorption and reactions with the H-ZSM-5 framework [22]. The differences between the cluster models are the termination of the connecting groups and the number of included tetrahedral molecules, for which significant effects of the cluster size on the protolytic cracking energetics have been reported [23]. For reducing the computational cost and minimizing the effect of the cluster size, the 12T cluster zeolite model was used in this work to mimic a part of a siliceous crystallographic H-ZSM-5 structure. This structure consists of one aluminum and eleven silicon tetrahedral units with the dangling bonds resulting from the termination of the Si-O bonds saturated by hydrogen atoms with a fixed Si-H bond distance of 1.47 Å, as shown in Fig. 1.

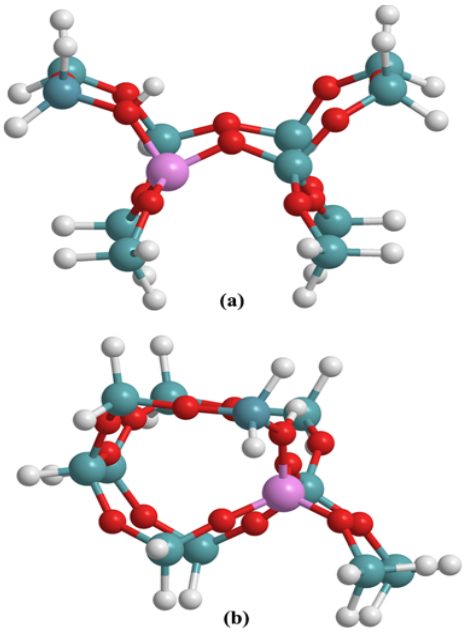

Fig. 1. 12T cluster represents the pore structure of H-ZSM-5 in (a) straight view and (b) side view.

2.2 Electronic structure calculation methods

Recently, the meta-hybrid M06 density functional has been used to yield intermolecular geometries for adsorption on zeolites similar to those of MP2 calculations, and M06-2X is an ideal choice for the treatment of molecular adsorption over zeolites [24]. Hence, M06-2X, which includes a mixture of Hartree-Fock exchange with DFT exchange-correlation, was used for all the calculations in this work. To obtain more accurate interaction energies, the 6-311++G(d, p) basis set with polarization functions added to all the atoms was employed. The geometry optimizations, vibrational frequencies, and energy calculations were conducted at the M06-2X/6-311++G(d, p) level of theory. The transition states corresponding to desired reaction coordinates were identified by the imaginary frequencies analysis and visual inspections. For ambiguous cases, the intrinsic reaction path analysis was utilized to examine the connections of each saddle point to its local minima. All of the calculations were performed with the Gaussian 09 package [25].

2.3 Kinetic theory

The reaction mechanism consists of at least one reaction for reactant adsorption, whose rates are

of extreme importance for heterogeneous catalysis [26]. In this work, the catalytic pyrolysis of MA is approximated as

$$\mathrm{MA} + \text{H-ZSM-5} \rightleftharpoons \text{MA-H-ZSM-5} \rightarrow \text{Products} \quad \text{(E1)}$$

where the rate coefficients for the adsorption, desorption and chemical reaction are k_I, k_{-I} and k_{II}, the concentration of MA and reaction sites of catalysts were denoted as the C_{MA} and C_{ZSM}. With the steady-state approximation applied to MA-H-ZSM-5, the simplified global reaction rate is given by

$$\mathrm{r} = \frac{k_I k_{II} C_{MA} C_{ZSM}}{k_I C_{MA} + k_{-I} + k_{II}} \quad \text{(E2)}$$

For the chemical reaction with a pronounced transition state, the conventional transition state theory was employed for the rate coefficient expressed by [27]:

$$\mathrm{k(T)} = \kappa \frac{k_B}{h} \frac{Q_{TS}}{\prod_i Q_i} \exp\left(\frac{-E_0}{k_B T}\right) \quad \text{(E3)}$$

$$\kappa = 1 + \frac{1}{24}\left(\frac{-h\nu^{\neq}}{k_B T}\right)^2 \quad \text{(E4)}$$

$$\mathrm{Q} = Q_{tra} Q_{vib} Q_{rot} Q_e \quad \text{(E5)}$$

where Q, k_B, h, E_0 and T are the partition function, Boltzmann constant, Planck constant, barrier height, and temperature. Wigner's tunneling correction is represented by κ, and $\nu^{\neq}$ is the imaginary frequency of the transition state. Q_{tra}, Q_{vib}, Q_{rot} and Q_e are the partition functions of the translational, vibrational, rotational, and electronic degrees of freedom. It is noted that the translational degrees of freedom are the same for the transition state and the reactants in the present problem.

3. Results and discussion

3.1 Adsorption of MA on H-ZSM-5 zeolites

In its decomposition reactions over the zeolites, MA adsorbs at the Bronsted acid site (O1-H1) of H-ZSM-5 through the formation of an O-H1 hydrogen bond. Fig. 2 shows the optimized geometries of two conformations for the adsorbed MA on the H-ZSM-5 zeolites, which have

different O atoms in the hydrogen bond. As shown in Fig. 2(a), the hydrogen bond interaction between O3 and proton H1 results in the adsorption of MA on the zeolite, denoted as Ads_MA1. As predicted, the molecular plane of the COO in the Ads_MA1 is perpendicular to that of H-O1-Al, which is conducive to the formation of its hydrogen bond. Fig. 2(b) shows the optimized geometry of the Ads_MA2, in which the hydrogen bond is formed between the proton H1 and O4 atom of methoxy group on MA. The atomic distance of H1-O4 is 1.50 Å, which is longer than that of Ads_MA1 by 0.09 Å, indicating a looser hydrogen bond interaction in Ads_MA2. The adsorption energy of MA producing Ads_MA1 and Ads_MA2 are 23.1 kcal/mol and 19.8 kcal/mol respectively, in which the tighter hydrogen bond interaction in Ads_MA1 cause the adsorption energy higher than that of Ads_MA2.

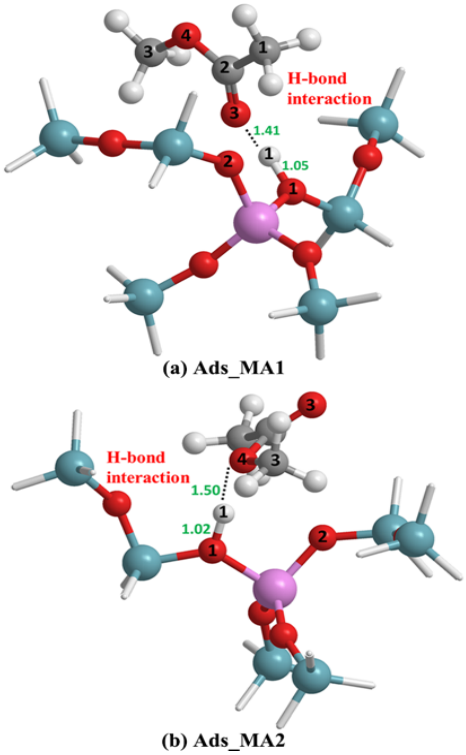

Fig. 2. Optimized structures of (a) Ads_MA1, MA adsorption through H1-O3 hydrogen bond, and (b) Ads_MA2, MA adsorption through H1-O4 hydrogen bond.

3.2 Potential energy surface

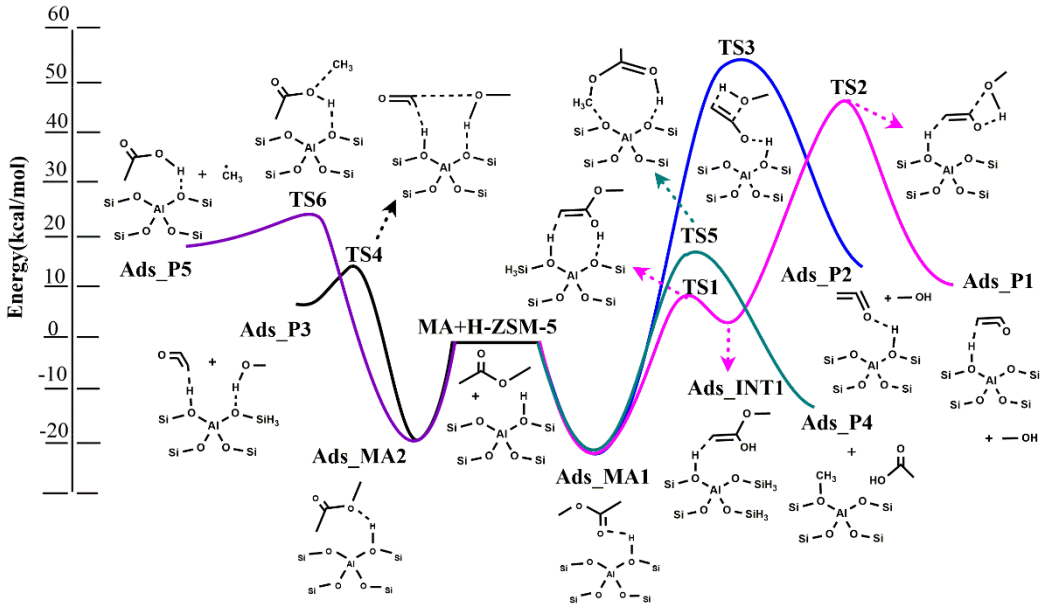

Fig. 3. Potential energy surface of the catalytic pyrolysis reactions of MA at the M06-2X/6-311++G(d, p) level.

The C-O and C-C bonds of the adsorbed MA crack leading to the products interacting with the zeolites. All of the possible reaction channels were investigated in this work. For clarity and simplicity, only the energetically favorable reactions are shown in Fig. 3, where the sum of energies of a separate MA molecule and the H-ZSM-5 zeolite is set as the reference energy.

Ketene, the first generation of highly reactive intermediates and synthons in organic chemistry, and a critical intermediate in the catalytic synthesis of hydrocarbon and olefins, was identified as a product of MA pyrolysis. The stepwise and concerted mechanisms were proposed to elucidate the formation of ketene in the present work for the MA pyrolysis. Fig. 4 illustrates the optimized structure of important species involved in the formation of ketene and methanol in the stepwise mechanism and those in the concerted mechanism. In the stepwise mechanism, Ads_MA1 undergoes the hydrogen exchange producing Ads_INT1 via an 8-membered-ring transition state (TS1) with the relative energy of 6.8 kcal/mol. Subsequently, Ads_INT1 dissociates to ketene and methanol through the cleavage of the C2-O4 bond with the relative energy of 48.7 kcal/mol, which is significantly

higher than that of the hydrogen exchange step and thus believed to be the rate-limiting step. In the concerted mechanism, it is shown that ketene can be generated from either Ads_MA1 or Ads_MA2 through a single step. Ads_MA1 undergoes 4-membered intramolecular hydrogen transfer, and the C2-O4 bond breaks via a transition state (TS3) with a relative energy of 53.5 kcal/mol and TS3 is stabilized at the active site of H-ZSM-5 by the O3-H1 hydrogen bond. Unlike for the reaction from Ads_MA1 in the concerted mechanism, the ketene was formed from Ads_MA2 through an 8-membered intermolecular exchange transition state (TS4) with the relative energy of 23.6 kcal/mol. The activation energy of TS4 is much lower than that of TS3 by 33.2 kcal/mol, because of the stronger electron interaction in TS4 consisting of the π-H interaction and the O1-H1 hydrogen bond. It can be concluded that the concerted decomposition reaction from the Ads_MA2 is one of most competitive reactions to produce the ketene. And Fig. 4(c) depicts the optimized geometries for the transition state (TS4) for the decomposition of Ads_MA2 in the concerted mechanism. In the transition state, the acidic proton H1 of the lattice move toward the O4 atom of MA and the H2 atom of the C1 group vibrates to access the O2 atom bonded to the Al atom in a single step. Meanwhile, the breaking of the C2-O4 bond results in ketene formation. Instantaneous protonation and deprotonation of MA is achieved through the hydrogen bond interactions formed between O1-H1 and O2-H2, along with the π-H interactions between the H2 atom and the π delocalization.

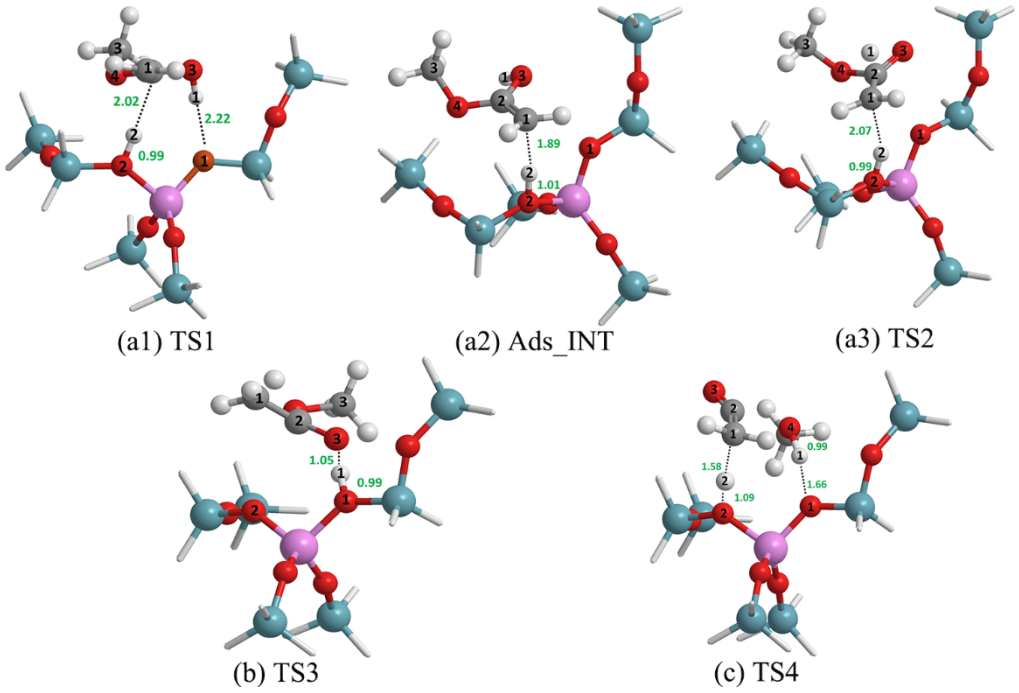

Fig. 4. Optimized structures of the transition states and the intermediate involved in the formation of the methanol and ketene from (a) the Ads_MA1 in stepwise mechanism, (b) from Ads_MA1 in concerted mechanism, and (c) from Ads_MA2 in concerted mechanism.

In addition, the catalytic cracking of MA is proposed to occur via a monomolecular mechanism in which the reaction proceeds through a carbonium ion as its transition state. Subsequently, the carbonium ion formed by the direct pronation of the Bronsted acid to MA collapses, leading to scissions of weak bonds to generate lighter products. Since the C3-O4 bond is weak, the highly reactive $CH_3C(=OH)OCH_3$ intermediate decomposed to acetic acid and the adsorbed methoxyl species through the breaking of the C3-O4 bond without energy barriers. For the channels through TS5, the adsorbed CH_3COOH and methoxy species bonded to the zeolites are produced from the protolytic cracking at the C3-O4 bond of MA with an energy barrier of 41.6 kcal/mol, which is more energetically favorable than that of protolytic cracking at the C1-C2 bond of MA by 31.9 kcal/mol. For the channels through TS6, the carbonium ion is generated directly by the Bronsted H1 proton bond to C4 and then decomposes presumably to the CH_3COO and CH_3 radicals with the activation energy of 43.3 kcal/mol, which is comparable to that of TS5.

3.3 High-pressure limit rate coefficients

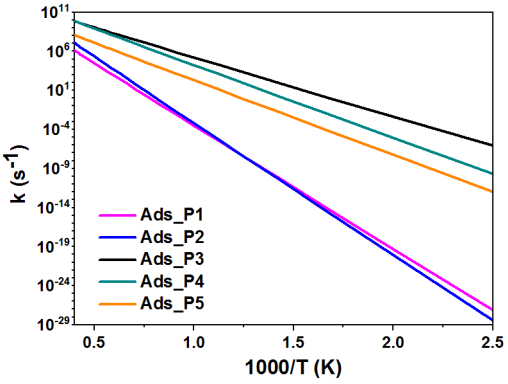

Fig. 5. High-pressure limit rate coefficients of main reactions in the MA catalytic pyrolysis.

High-pressure limit rate coefficients of isomerization and decomposition reactions in the catalytic pyrolysis of MA are displayed in Fig. 5, and their fitted Arrhenius expressions are listed in Table 1. It is noted that the rate coefficients of the reactions forming the Ads_P1 were derived using the steady-state approximation, in which k_1 is the rate constant of reactions from Ads_MA1to Ads_INT and k_2 is that of reactions connecting the Ads_INT with Ads_P1. For the multi-step reactions from Ads_MA1 to the ketene formation, where the $k_1 >> k_2$, thus its reaction constant expressed as follows:

$$\mathrm{k} = \frac{k_1 k_2}{k_{-1}+k_2} \qquad \text{(E6)}$$

It is seen that the reaction generating the Ads_P3 (ketene + methanol) is the most favorable reactions since it has the lowest energy barrier, and that the reaction leading to the Ads_P4 (CH_3 + CH_3COO) is secondary. Because of its higher barrier height, Ads_MA1 decomposition to Ads_P2 in a single step shows less reactivity. The main products are ketene + methanol and CH_3 + CH_3COO. Overall, the reactions to Ads_P3 (ketene + methanol) account for more than 50% consumption of MA at low and intermediate temperatures.

Table 1. Rate constants k(T) and change of Gibbs free energy (ΔG) of key reactions for MA catalytic pyrolysis [a]

Reactions	A	n	E	ΔG
Ads_MA1→Ads_INT1(TS1)	2.97E+12	-0.08	31.28	29.48
Ads_INT1→Ads_P1(TS2)	1.58E+13	0.00	44.93	4.24
Ads_MA1→Ads_P1(Overall)	3.61E+12	-0.11	31.36	33.73
Ads_MA1→Ads_P2(TS3)	3.41E+13	0.12	78.46	42.36
Ads_MA2→Ads_P3(TS4)	3.98E+12	0.10	35.32	30.81
Ads_MA1→Ads_P4(TS5)	5.80E+13	-0.04	43.05	13.65
Ads_MA2→Ads_P5(TS6)	1.57E+10	0.45	42.04	37.84

[a] units of A, E and ΔG are s^{-1}, kcal mol^{-1} and kcal mol^{-1}, respectively. $k(T)= AT^n \exp(-E_a/RT)$.

3.4 Comparisons with the gas-phase pyrolysis of MA

To illustrate the superiority of the catalytic pyrolysis over the gas-phase pyrolysis of MA, potential energy surfaces of both the gas-phase pyrolysis and catalytic pyrolysis of MA are compared in Fig. 6.

The reaction scheme of the four primary dissociation reaction channels for MA is shown in Fig. 6. The energy barrier for the ketene and methanol formation through the single transition state is 72.0 kcal/mol, in a good agreement with that calculated at the CCSD(T)//cc-pv∞z//B3LYP/6-311++G(d,p) level of theory by Peukert et al. [11]. Additionally, the ketene and methanol can also be produced through a two-step reaction. First, a hydrogen atom is transferred from the methyl group to the oxygen atom of the carbonyl group through a four-membered-ring transition state with the energy barrier of 70.5 kcal/mol, leading to the generation of the MA enol isomer (CH_2=C(OH)OCH_3) intermediate. Then, CH_2=C(OH)OCH_3 dissociates to the ketene and methanol through a β-scission reaction with the transition state energy of 69.2 kcal/mol. The other two important reaction channels proceed through the direct cleavage of the C-O bond via a barrier-less reaction that leads to the formation of CH_3 + C(=O)OCH_3 and CH_3C(=O)O + CH_3, for which the relative energies are 93.4 kcal/mol and 88.2 kcal/mol, respectively.

It is seen that the overall activation energies in the catalytic pyrolysis are considerably lower

than those in the gas-phase pyrolysis of MA. The overall energy barrier of TS4 is 13.8 kcal/mol, which is lower than that in the direct pyrolysis by 58.2 kcal/mol. For reactions in the stepwise mechanism, the isomerization step in the catalytic pyrolysis of MA with activation energy of 6.8 kcal/mol is more energetically favorable than that in the direct pyrolysis of MA by 53.6 kcal/mol. The monomolecular C-O bond breaks through an apparent transition state TS5 with the energy of 18.5 kcal/mol and is much more energetically favorable than the barrierless reaction producing the acetyloxy + CH_3 with the energy barrier of 88.2 kcal/mol. The energy barriers of the dissociation reactions for MA over H-ZSM-5 zeolites decrease significantly due to the electronic interaction between MA and the Bronsted proton within the zeolite pore. The significant activation energy decrease effectively leads to the reduction in the pyrolysis temperature, which is environmentally friendly for the VOC controlling. The branching ratios between these radical channels and molecular product channels have a strong influence on the radicals available to a combustion process. According to branching ratios obtained by Peukert et al. [11], the methyl carbonyl produced in the reaction occupies approximately 87% of MA consumption. The acetyloxyl and direct ketene-forming reactions are the secondary products with the branching ratio of approximately 6%. In contrary, most of the MA over H-ZSM-5 zeolites is dissociated to yield ketene and methanol in a single step and the secondary production is the compounds of CH_3+ CH_3COO.

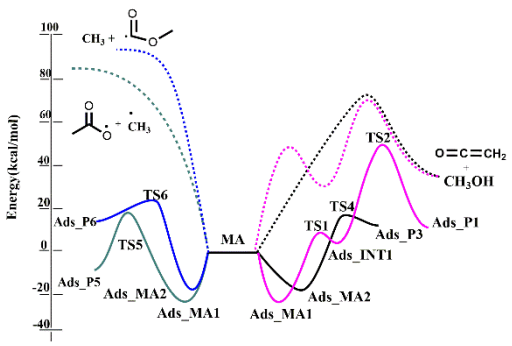

Fig. 6. Potential energy surfaces consisting of selected favorable dissociation reactions for the conventional pyrolysis (dash lines) and the catalytic pyrolysis over H-ZSM-5 zeolites of MA (solid

lines).

4. Conclusions

Catalytic pyrolysis of MA has been investigated theoretically in the present work and its decomposition reactions were modeled using the 12T H-ZSM-5 cluster calculated at the M06-2X/6-311++G(d, p) level of theory. Kinetic parameters of chemical rate constants for the surface-solid reactions were obtained by using the transition state theory. Firstly, this study on the kinetic mechanisms of MA catalytic pyrolysis demonstrated that the ketene produced in the concerted mechanism and cracking reactions leading to the formation of acetyloxy + CH_3 provide the most competitive MA consumption channels and the branching ratios were also shown roughly for further comparisons. Secondly, compared+ to the gas-phase pyrolysis of MA, the energy barriers of the corresponding reactions in the catalytic pyrolysis decrease considerably, which cut off the reaction temperatures and that is the key for the efficient combustion and pollution controlling, demonstrating the superiority of the catalytic pyrolysis in MA. In addition, the ketene becomes the main dissociation product instead of the methyl radicals. And lastly, ketene, the curious case in zeolite chemistry and catalysis, is the main product of MA catalytic pyrolysis. As ketenes have great influence on controlling selectivity of important zeolite-catalyzed process, explicit discussions were made on the stepwise and the concerted mechanisms of the ketene formation. The present reaction mechanism of MA over H-ZSM-5 zeolites provides guidance for the catalytic combustion behavior of biodiesels, will promote the mechanism development of ketene-selecting catalytic conventions, and extends kinetic data for VOC processing.

Acknowledgements

The work at University of Science and Technology of China was supported by Natural Science Foundation of China (51676176, 11575178 and U1532137) and Fundamental Research Funds for the

Central Universities (WK2320000038). The work at the Hong Kong Polytechnic University was supported by NSFC (No. 91641105) and the university matching fund (4-BCE8).

References:

[1] K. Kohse-Hoinghaus, P. Osswald, T.A. Cool, T. Kasper, N. Hansen, F. Qi, C.K. Westbrook, P.R. Westmoreland, Biofuel combustion chemistry: from ethanol to biodiesel, Angew. Chem. Int. Ed. Engl., 49 (2010) 3572-3597.

[2] J.Y.W. Lai, K.C. Lin, A. Violi, Biodiesel combustion: Advances in chemical kinetic modeling, Prog. Energy Combust. Sci., 37 (2011) 1-14.

[3] B. Akih-Kumgeh, J.M. Bergthorson, Structure-reactivity trends of C1-C4 alkanoic acid methyl esters, Combust. Flame, 158 (2011) 1037-1048.

[4] W. Ren, K.-Y. Lam, D.F. Davidson, R.K. Hanson, X. Yang, Pyrolysis and oxidation of methyl acetate in a shock tube: A multi-species time-history study, Proc. Combust. Inst. 36 (2017) 255-264.

[5] C.K. Westbrook, W.J. Pitz, P.R. Westmoreland, F.L. Dryer, M. Chaos, P. Oßwald, K. Kohse-Höinghaus, T.A. Cool, J. Wang, B. Yang, A detailed chemical kinetic reaction mechanism for oxidation of four small alkyl esters in laminar premixed flames, Proc. Combust. Inst., 32 (2009) 221-228.

[6] X. Yang, D. Felsmann, N. Kurimoto, J. Krüger, T. Wada, T. Tan, E.A. Carter, K. Kohse-Höinghaus, Y. Ju, Kinetic studies of methyl acetate pyrolysis and oxidation in a flow reactor and a low-pressure flat flame using molecular-beam mass spectrometry, Proc. Combust. Inst., 35 (2015) 491-498.

[7] Q. Meng, X. Zhao, L. Zhang, P. Zhang, L. Sheng, A theoretical kinetics study on low-temperature reactions of methyl acetate radicals with molecular oxygen, Combust. Flame, 196 (2018) 45-53.

[8] C.N. R. S, Methyl Acetate Oxidation in a JSR: Experimental and Detailed Kinetic Modeling Study, Combust. Sci. Technol., 127 (1997) 275-291.

[9] E.J. Hintsa, A.M. Wodtke, Y.T. Lee, Infrared multiphoton dissociation of ethyl and methyl acetate, J. Phys. Chem., 92 (1988) 5379-5387.

[10] K. Sulzmann, D. Baxter, M. Khazra, T. Lund, Initiation of methyl acetate pyrolysis in argon-diluted mixtures behind reflected shock waves, J. Phys. Chem., 89 (1985) 3561-3566.

[11] S.L. Peukert, R. Sivaramakrishnan, M.C. Su, J.V. Michael, High temperature rate constants for H/D+methyl formate and methyl acetate, Proc. Combust. Inst., 34 (2013) 463-471.

[12] A. Farooq, D. Davidson, R. Hanson, L. Huynh, A. Violi, An experimental and computational study of methyl ester decomposition pathways using shock tubes, Proc. Combust. Inst., 32 (2009) 247-253.

[13] C.J. Annesley, C.F. Goldsmith, R.S. Tranter, A shock tube laser schlieren study of methyl acetate dissociation in the fall-off regime, Phys. Chem. Chem. Phys., 16 (2014) 7241-7250.

[14] Y. Liu, S. Muller, D. Berger, J. Jelic, K. Reuter, M. Tonigold, M. Sanchez-Sanchez, J.A. Lercher, Formation Mechanism of the First Carbon-Carbon Bond and the First Olefin in the Methanol Conversion into Hydrocarbons, Angew. Chem. Int. Ed. Engl., 55 (2016) 5723-5726.

[15] A.D. Chowdhury, A.L. Paioni, K. Houben, G.T. Whiting, M. Baldus, B.M. Weckhuysen, Bridging the Gap between the Direct and Hydrocarbon Pool Mechanisms of the Methanol-to-Hydrocarbons Process, Angew. Chem. Int. Ed. Engl., 57 (2018) 8095-8099.

[16] D.B. Rasmussen, J.M. Christensen, B. Temel, F. Studt, P.G. Moses, J. Rossmeisl, A. Riisager, A.D. Jensen, Ketene as a Reaction Intermediate in the Carbonylation of Dimethyl Ether to Methyl Acetate over Mordenite, Angew. Chem. Int. Ed. Engl., 54 (2015) 7261-7264.

[17] L. Xu, Y. Xu, Activation of methyl acetate on Pd(111), Surf. Sci., 604 (2010) 887-892.

[18] T. Romotowski, J. Komorek, Some aspects of interactions of methanol, acetic acid, and methylacetate with

HNaZSM-5 zeolite, Zeolites, 11 (1991) 35-41.
[19] N. Chen, D. Walsh, L. Koenig, Fluidized bed upgrading of wood pyrolysis liquids and related compounds, Prepr. Pap., Am. Chem. Soc., Div. Fuel Chem.;(United States), 32 (1987).
[20] T.A. Semelsberger, K.C. Ott, R.L. Borup, H.L. Greene, Generating hydrogen-rich fuel-cell feeds from dimethyl ether (DME) using Cu/Zn supported on various solid-acid substrates, Appl. Catal. A-Gen, 309 (2006) 210-223.
[21] P.M. Zimmerman, D.C. Tranca, J. Gomes, D.S. Lambrecht, M. Head-Gordon, A.T. Bell, Ab initio simulations reveal that reaction dynamics strongly affect product selectivity for the cracking of alkanes over H-MFI, J. Am. Chem. Soc., 134 (2012) 19468-19476.
[22] S. Svelle, C. Tuma, X. Rozanska, T. Kerber, J. Sauer, Quantum chemical modeling of zeolite-catalyzed methylation reactions: toward chemical accuracy for barriers, J. Am. Chem. Soc., 131 (2008) 816-825.
[23] Y. Horbatenko, J.P. Pérez, P. Hernández, M. Swart, M. Solà, Reaction Mechanisms for the Formation of Mono- And Dipropylene Glycol from the Propylene Oxide Hydrolysis over ZSM-5 Zeolite, J. Phys. Chem. C, 118 (2014) 21952-21962.
[24] Y. Zhao, D.G. Truhlar, Benchmark data for interactions in zeolite model complexes and their use for assessment and validation of electronic structure methods, J. Phys. Chem. C, 112 (2008) 6860-6868.
[25] M. Frisch, G. Trucks, H.B. Schlegel, G. Scuseria, M. Robb, J. Cheeseman, G. Scalmani, V. Barone, B. Mennucci, G. Petersson, Gaussian 09, revision a. 02, gaussian, Inc., Wallingford, CT, 200 (2009).
[26] S.J. Klippenstein, V.S. Pande, D.G. Truhlar, Chemical Kinetics and Mechanisms of Complex Systems: A Perspective on Recent Theoretical Advances, J. Am. Chem. Soc., 136 (2014) 528-546.
[27] D.G. Truhlar, B.C. Garrett, Variational transition state theory, Annu. Rev. Phys. Chem., 35 (1984) 159-189.

List of Figure captions

Fig. 1. 12T cluster represents the pore structure of H-ZSM-5 in (a) straight view and (b) side view.

Fig. 2. Optimized structures of (a) Ads_MA1, MA adsorption through H1-O3 hydrogen bond, and (b) Ads_MA2, MA adsorption through H1-O4 hydrogen bond.

Fig. 3. Potential energy surface of the catalytic pyrolysis reactions of MA at the M06-2X/ 6-311++ G(d, p) level.

Fig. 4. Optimized structures of the transition states and the intermediate involved in the formation of the methanol and ketene from (a) the Ads_MA1 in stepwise mechanism, (b) from Ads_MA1 in concerted mechanism, and (c) from Ads_MA2 in concerted mechanism.

Fig. 5. High-pressure limit rate coefficients of main reactions in the MA catalytic pyrolysis.

Table 1. Rate constants k(T) and change of Gibbs free energy (ΔG) of key reactions for MA catalytic pyrolysis.

Fig. 6. Potential energy surfaces consisting of selected favorable dissociation reactions for the conventional pyrolysis (dash lines) and the catalytic pyrolysis over H-ZSM-5 zeolites of MA (solid lines).

Two Supplemental Materials

Table S1. Geometric parameters of transition states for the catalytic cracking of MA at C1-C2 bond over H-ZSM-5 zeolites[a]

Table S2. Geometric parameters of species for the ketene formation of MA over H-ZSM-5 zeolites in the stepwise mechanism[a].

Table S3. Geometric parameters of transition states and products for the ketene formation of MA over H-ZSM-5 zeolites in the concerted mechanism [a]

Table S4. Geometric parameters of transition states and products for acetyloxy and CH_3 formation of MA over H-ZSM-5 zeolites[a]

Fig. S1. Optimized structures of all species for the protolytic cracking of MA from Ads_MA1 at the C1-C2 bond. (a) The adsorbed transition state of the intermolecular hydrogen transfer from the zeolites to C1 atom, links to the formation of (b) adsorbed methane and methoxy carbonyl. Only the 5T active region within the H-ZSM-5 is displayed for clarity.

Fig. S2. Optimized structures of the transition states of the protolytic cracking of MA at C3-O4 bond from (a) the Ads_MA1 and (b) the Ads_MA2.

Fig. S3. Optimized structures of all species for the protolytic cracking of MA from Ads_MA1 at the C1-C2 bond. (a) The adsorbed transition state of the intermolecular hydrogen transfer from the zeolites to C1 atom, links to the formation of (b) adsorbed methane and methoxy carbonyl.

Fig. S4. Optimized structures of the products involved in the protolytic cracking of MA at C3-O4 bond from (a) the Ads_MA1 and (b) the Ads_MA2 in monomolecular mechanism.

Cartesian coordinates for all the stationary points and transition states in all the reaction paths with the 12T H-ZSM-5